

# Multi-normal-mode splitting of a cavity in the presence of atoms – towards the superstrong coupling regime

Xudong Yu<sup>1</sup>, Dezhi Xiong<sup>1</sup>, Haixia Chen<sup>1</sup>, Pengjun Wang<sup>1</sup>, Min Xiao<sup>1,2</sup>, Jing Zhang<sup>1†</sup>

<sup>1</sup>*The State Key Laboratory of Quantum Optics and Quantum Optics Devices,*

*Institute of Opto-Electronics, Shanxi University, Taiyuan 030006, P.R. China and*

<sup>2</sup>*Department of Physics, University of Arkansas, Fayetteville, Arkansas 72701, USA*

Multi-normal-mode splitting peaks are experimentally observed in a system with Doppler-broadened two-level atoms inside a relatively long optical cavity. In this system, the atoms-cavity interaction can reach the “superstrong coupling” condition with atoms-cavity coupling strength  $g\sqrt{N}$  to be near or larger than the cavity free-spectral range  $\Delta_{FSR}$ . In such case, normal-mode splitting can occur in many cavity longitudinal modes to generate the multi-normal-mode splitting peaks, which can be well explained by the linear dispersion enhancement due to the largely increased atomic density in the cavity. Many new interesting phenomena might come out of this superstrong atoms-cavity coupling regime.

Studies of strong coupling between atoms and cavity field have been very active in the past 30 years [1] due to its importance in the fundamental understanding of quantum electrodynamics and potential applications in quantum computation and quantum information processing [2]. In the traditional cavity-quantum electrodynamics (C-QED), high finesse microcavities are normally used to enhance the single-photon coupling strength  $g$  ( $= \sqrt{\frac{\mu^2 \omega_c}{2\hbar V_M}}$ , where  $\omega_c$  is the resonant frequency of the cavity,  $\mu$  is the atomic dipole matrix element,  $V_M$  is the cavity mode volume), so the strong-coupling condition of  $g > \kappa, \gamma$  can be satisfied even with a single atom [1, 3, 4] (where  $\kappa$  is the cavity decay rate and  $\gamma$  is the atomic decay rate). Two normal-mode splitting peaks (i.e. Rabi sidebands) appear in the cavity transmission spectrum due to such strong atom-cavity interaction, with the frequency space between the two side peaks given by  $2g$ . This atom-cavity coupling strength  $g$  can be enhanced by using an assemble of atoms to be  $g\sqrt{N}$ , where  $N$  is the number of atoms in the cavity mode volume [5, 6]. Normal-mode splitting in assemble of two-level atoms has been demonstrated in atomic beams [7, 8], cold atomic cloud [9, 10, 11] and Bose-Einstein condensate [12]. Recently, such normal-mode splitting was even observed in Doppler-broadened two-level atoms in a hot atomic vapor cell inside a low finesse ring cavity [13].

A different regime of atoms-cavity interaction has been investigated in a system with cold atoms in an optical lattice formed inside a high-finesse, macroscopic optical cavity [9, 14, 15]. Interesting effects, such as cavity-mediated collective light scattering due to the self-organized atoms in the intracavity optical lattice and collective atomic motion, were observed in such system [15]. Recently, normal-mode splitting and collective mechanical effects have also been studied in such atoms-cavity system [9]. The coherent backscattering between the two propagating directions of a longitudinal mode has enhanced the coupling between the atoms in the optical lattice and the cavity fields, even when the fields are detuned far from the atomic resonance [15].

In this Letter, we present our experimental demonstration of multi-normal-mode splitting peaks due to strong coupling between high-density, inhomogeneously-broadened two-level

atoms and multiple longitudinal cavity modes in a long Fabre-Perot optical cavity. Here, we have reached a new regime of strong atoms-cavity interaction, i.e. with  $g\sqrt{N} > \Delta_{FSR}$ , where  $\Delta_{FSR}$  is the free-spectral range (FSR) of the optical cavity. Meiser and Meystre theoretically studied a system under such condition with a microscopic number of atoms [16] and named it as the “superstrong coupling” regime in the C-QED. Such superstrong coupling condition has not been reached in previous experiments due to either short optical cavity (therefore very large  $\Delta_{FSR}$ ) used to increase  $g$  or relatively low atomic density. In the current experimental system with inhomogeneously-broadened two-level atoms in a long optical cavity, the atomic density can be easily increased to satisfy this superstrong coupling condition. With normal-mode splittings for multiple longitudinal cavity modes, different cavity modes and their atom-cavity polaritons can interact with each other, which can provide the atom-mediated coupling between different cavity modes via  $\chi(3)$  nonlinearity [17]. Such coupling between different cavity field modes can be used for many applications in quantum information processing, such as phase gates and multimode entangled states. With such demonstrated new regime in atoms-cavity interaction, many more interesting applications can be envisioned, including ones in solid-state systems and photonic crystal cavities.

In the model of the coupled atoms-cavity system, the cavity is a standing-wave cavity with length  $L_c$ , and the intracavity medium is an assemble of two-level atoms, whose resonance frequency  $\omega_a$  is near a cavity resonance at frequency  $\omega_c$ . The two-level atomic medium has a length  $L_a < L_c$  with  $N$  atoms in the cavity volume. The intensity transmission function of a probe laser ( $\omega_L$ ) for this coupled atoms-cavity system can be easily found and is given by Eq.1 in Ref. [7]. The frequency-dependent intensity-absorption coefficient and the refractive index of the atomic medium are given by

$$\alpha = \alpha_0 \frac{\gamma_a^2}{4\Delta^2 + \gamma_a^2} \quad (1)$$

$$n = 1 - \alpha_0 \frac{c}{\omega_a} \frac{2\Delta\gamma_a}{4\Delta^2 + \gamma_a^2}, \quad (2)$$

respectively, where  $\alpha_0 = \omega_a N_D |\mu|^2 / \varepsilon_0 \hbar c \gamma_a$  is the line-center absorption coefficient. Notice that Eqs.1 and 2 are valid only when  $2\pi\alpha_0/\lambda_a \ll 1$  [18]. Here, the angle sustained by the cavity mode is small, and the transverse decay rate can be very closely approximated by the atomic free-space decay rate  $\gamma_a = \mu^2 \omega_a^3 / 3\pi \hbar \varepsilon_0 c^3$ . Thus, the line-center absorption coefficient becomes  $\alpha_0 = \frac{3\pi c^2}{\omega_a^2} N_D$ .  $\Delta = \omega_L - \omega_a$  and  $\Delta_{ac} = \omega_a - \omega_c$  are the laser-atom and atom-cavity frequency detunings, respectively. The cavity linewidth is given by  $\kappa = \Delta_{FSR}/F$ , where  $F$  is the cavity finesse. This linear-dispersion theory was used to explain the experimental observation in the system with a two-level atomic beam passing through an one-centimeter long standing-wave cavity [7], where only one cavity longitudinal mode ( $m=0$ ) was considered.

Here, we can also apply this linear-dispersion theory to the case with superstrong coupling, in which other cavity longitudinal modes ( $m = \pm 1$  and  $m = \pm 2$ , et al) have to be included. We will only consider the case of  $\Delta_{ac} = 0$ . For an empty cavity, the cavity transmission peaks are Lorentzian in shape and occur at  $\phi(\omega_L) = \pm m 2\pi$ , where  $\phi$  is the round-trip phase shift experienced by the intracavity field going through the cavity and  $m = 0, 1, 2, \dots$ , with equal mode spaces given by  $\Delta_{FSR}$ , as can be easily seen from the cavity transmission function (Eq. (1) in Ref. [7]). With an intracavity (two-level) atomic medium, the cavity transmission structure is significantly modified. First, when the atomic density is high enough, so  $g\sqrt{N} \gg \gamma_a, \kappa$ , but much smaller than  $\Delta_{FSR}$ ,  $\phi(\omega_L) = 0$  will have two real solutions due to the dispersion introduced by the atoms as given in Eq. (2). This indicates that the center peak ( $m=0$ ) in the cavity transmission is split into two side peaks located at  $\pm g\sqrt{N}$ , respectively, which is the standard normal-mode splitting, as shown in Fig. 1(a). Under this condition, the other cavity modes ( $m = \pm 1$  and  $m = \pm 2$ , et al) are not affected by the atoms and still have equal spaces between them given by  $\Delta_{FSR}$ . However, as the condition that  $g\sqrt{N}$  is near or larger than  $\Delta_{FSR}$  is satisfied, then not only the center cavity mode ( $m = 0$ ) has normal-mode splitting, other cavity modes (such as  $m = \pm 1$ ) will interact with the atoms and have their own normal-mode splitting peaks (i.e.  $\phi(\omega_L) = 2\pi$  or  $\phi(\omega_L) = -2\pi$  will also have two real solutions), as shown in Fig.1(b). The positions of their two normal-mode splitting peaks for  $|m| \geq 1$  locate in the two sides of the atomic resonant frequency and present asymmetric structure as shown in Fig. 1(b). To see this, let's consider only the  $m = 1$  cavity mode, which can be viewed as a mode with an effective cavity detuning of  $\Delta_{FSR}$ . As it interacts with atoms under the “superstrong coupling” condition, the Rabi sidebands become very asymmetric (due to large effective detuning), with one large peak on the right (near the original empty cavity peak position) of the atomic resonance and a smaller peak on the left of the atomic resonance (all labeled as “1” in Figs. 1(b)-1(d)). When the atomic density gets even higher, more cavity modes (such as  $m = \pm 2$  and  $m = \pm 3$ , et al) will participate in the mode-splitting process, which form

the multi-normal-mode splitting structure, as shown in Figs. 1(c) and 1(d).

For our experimental situation, we consider a system with two-level rubidium atoms (in a vapor cell) inside an optical standing-wave cavity of 17.7 cm long. Here,  $\gamma_a = 2\pi \times 6 MHz$ . The original normal-mode splitting  $g\sqrt{N}$  can reach and even be larger than  $\Delta_{FSR}$  by increasing the temperature of the atomic cell (the corresponding atomic density is increased quickly with temperature). Due to Doppler effect, the absorption (and therefore also the dispersion) profile is much broader with a width of  $\delta\omega_D = \frac{\omega_a}{c} \sqrt{\frac{2k_B T}{m}}$ . For simplicity in discussion, we can replace the homogeneous absorption linewidth  $\gamma_a$  by the Doppler width  $\delta\omega_D$  in Eqs. 1 and 2, which is approximately valid. At the same time, the line-center absorption coefficient is changed into  $a_0 = \frac{3\pi c^2}{\omega_a^2} \frac{\gamma_a}{\omega_D} N_D$ . In order to accurately calculate the absorption and dispersion properties in the Doppler-broadened atomic system, we need to replace Eqs.1 and 2 by Eqs.5 and 6 of Ref.[13]. Notice that the second-term in the index of refraction of the intracavity medium (Eq. 2) depends on the atomic density in the cavity ( $a_0 \propto N_D$ ). So, as the temperature of the atomic cell increases, more cavity modes will participate in the mode-splitting interactions to generate the multi-normal-mode splitting peaks.

Parameters used in plotting Fig. 1 are basically the same as in our experiment. For very low absorption coefficient  $a_0$  (corresponding to low temperature or atomic density), the Doppler absorption and dispersion width ( $\delta\omega_D = 2\pi \times 343 MHz$ ) is smaller than the cavity free-spectral range ( $\Delta_{FSR} = 2\pi \times 850 MHz$ ). Therefore, except for the two middle normal-mode peaks, all other peaks are the cavity transmission peaks without mode-splitting (corresponding to Fig. 1(a)), since they do not interact strongly with the atoms. The shorter transmission peak height of the two middle normal-mode peaks is due to the atomic absorption. As the absorption coefficient  $a_0$  gets larger (higher temperature), the dispersion changes and more FSR cavity modes join the mode-splitting interactions, as shown in Figs. 1(b)-1(d). Figures 1(e) and 1(f) (which are the re-plots of Figs.1(b) and (d), respectively, with the FSR cavity mode number  $m$  as the horizontal axis) give a more clear insight into the positions and heights of the multi-normal-mode splitting peaks. Such plots are the typical avoided-crossing plots commonly used in cavity-QED.

The experiment was done using a standing-wave cavity of 17.7 cm long, as shown in Fig.2. The cavity composes of two mirrors with same radius of curvature of 100 mm. The reflectivity is 90% at 780 nm for the input coupler  $M1$ , which is mounted on a PZT to adjust the cavity length. The output coupler  $M2$  has a reflectivity of 99.5% at 780 nm. The finesse of the cavity including the losses of two faces of the atomic cell is about  $F = 20$ . The length of the vapor cell is 5 cm. The temperature of the vapor cell can be controlled by a heater. A grating-stabilized diode laser, which first passes a standard polarization maintaining single-mode fiber, was used as the cavity input beam with an input power of 4 mW. The

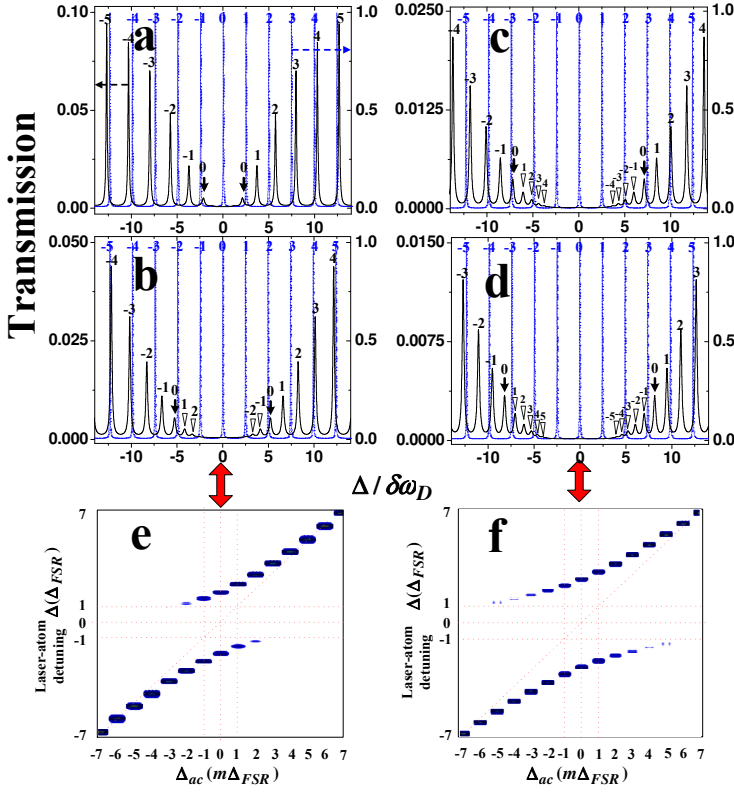


FIG. 1: (Color online). Theoretical calculations of the transmission spectra of the coupled atoms-cavity system with the Doppler-broadened two-level atoms with different absorption coefficients. For comparison, the cavity transmission spectrum for the empty cavity (blue dashed) is plotted in (a), (b), (c) and (d). The vertical scale is normalized to the light intensity transmitted through the empty cavity. This is for an optical cavity with  $\Delta_{FSR} = 2\pi \times 850$  MHz.  $m = 0, \pm 1, \pm 2, \dots$  label the multi-normal-mode splitting peaks coming from the FSR cavity modes. The finesse of the empty cavity  $F = 20$  and  $\lambda = 780$  nm. (a)  $a_0 L_a = 12$  (corresponding to  $N_D L_a = 9.4 \times 10^{15}/m^2$ ); (b)  $a_0 L_a = 70$  ( $N_D L_a = 5.5 \times 10^{16}/m^2$ ); (c)  $a_0 L_a = 130$  ( $N_D L_a = 1.0 \times 10^{17}/m^2$ ); (d)  $a_0 L_a = 170$  ( $N_D L_a = 1.3 \times 10^{17}/m^2$ ); (e) and (f) are the re-plots of (b) and (d), respectively.

laser beam with the spatial mode filter by an optical fiber is easier to mode-match to the  $TEM_{00}$  mode of the optical cavity. The diode laser has also been divided into several parts to be used in the saturated absorption spectroscopy (using another rubidium atomic cell) and in the F-P cavity for monitoring the frequency and mode of the laser. The optical cavity length was kept unchanged and the input laser frequency was scanned to measure the transmission spectra. The transition between the  $5S_{1/2}$ ,  $F = 1$  and  $5P_{3/2}$ ,  $F'$  in  $^{87}\text{Rb}$  was used for the two-level system.

At a low atomic cell temperature ( $T = 105^\circ\text{C}$ , corresponding to  $N_D L_a = 2.5 \times 10^{17}/m^2$  [19]), the cavity transmission spectrum is given in Fig.3(a). At both sides of the resonant frequency of atoms, the atoms-cavity normal modes can be observed. Only two normal-mode splitting peaks appear in the

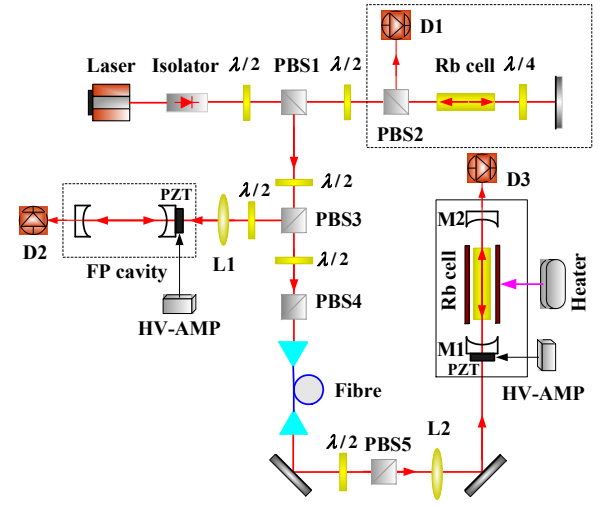


FIG. 2: (Color online). Schematic of the experimental setup of the coupled atoms-cavity system.  $\lambda/2$ : half-wave plate; D1, D2, D3: detectors; HV-AMP: high voltage amplifier; PZT: piezoelectric transducer; PBS: polarized beam splitter; L1, L2: optical lens.

transmission spectrum, and the other outside peaks are simply the cavity FSR peaks without mode-splitting, as predicted in Fig.1(a). Notice that the atomic density predicted theoretically in Fig.1(a) is about an order of magnitude smaller than the density predicted by Ref. [19] for rubidium at  $T = 105^\circ\text{C}$ , which is mainly due to a large fraction of atoms populated at  $5S_{1/2}$ ,  $F = 2$  when without a pump light [20]. As the temperature increases ( $T = 110^\circ\text{C}$ ), more FSR cavity modes participate in the mode-splitting process and generate the multi-normal-mode splitting peaks, as shown in Fig.3(b), which also agrees with the theoretical curve of Fig.1(b). In order to label the two original normal-mode splitting peaks, we must monitor the peaks carefully by slowly increasing the temperature. The asymmetry in the two transmission side peaks compared with Fig.1 is due to the influence of absorption from  $5S_{1/2}$ ,  $F = 2$  to  $5P_{3/2}$ ,  $F'$  transition in  $^{85}\text{Rb}$ , as shown in Fig.3(e). As the temperature is further increased ( $T = 115^\circ\text{C}$  and  $T = 120^\circ\text{C}$ ), more FSR cavity modes join in the mode-splitting interactions as shown in Figs.3 (c) and (d) (which are also predicted in Figs.1(c) and 1(d)) due to the largely increased dispersion as indicated by Eq.2. Since the atomic density (and therefore the absorption coefficient  $a_0$ ) depends exponentially on the temperature, the dispersion change (and therefore the number of FSR cavity modes generating multi-normal-mode splitting) has a very sensitive dependence on the temperature of the atomic cell, as shown in Fig.3.

In summary, we have studied the cavity transmission spectra in a system with Doppler-broadened two-level atoms in a standingwave cavity under the “superstrong coupling” condition of  $g\sqrt{N}$  larger or equal to  $\Delta_{FSR}$ . In this superstrong atoms-cavity coupling region, mode-splitting occurs in many FSR cavity modes due to the interactions with the intracavity Doppler-broadened atoms, and multi-normal-mode split-



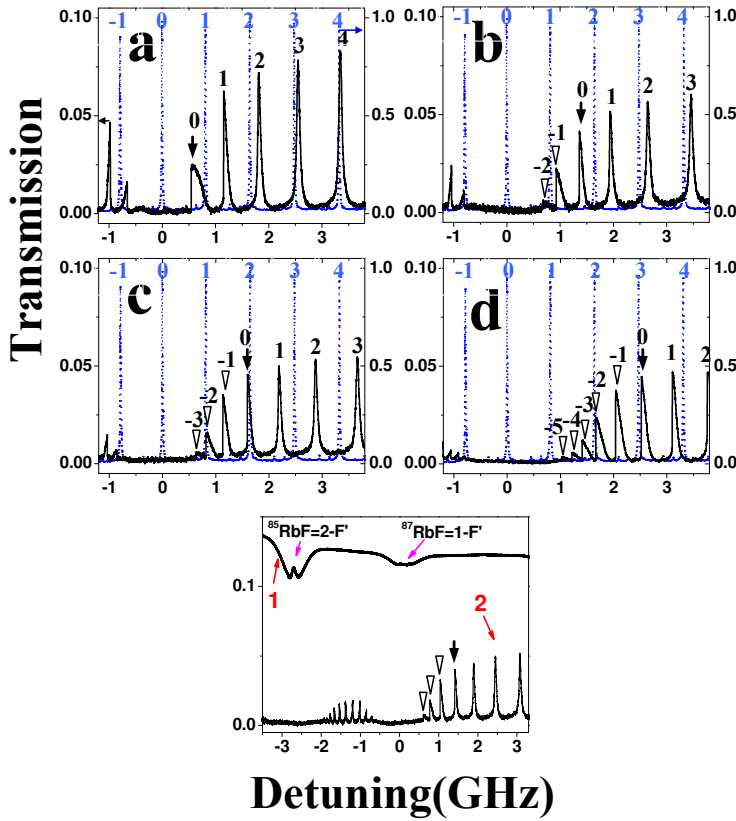


FIG. 3: (Color online). Experimentally measured transmission spectra of the coupled atoms-cavity system with the Doppler-broadened two-level atoms at different temperatures of the atomic cell. The curves (a), (b), (c) and (d) correspond to (e) with a narrow frequency detuning range. For comparison, the cavity transmission spectrum for the empty cavity (blue dashed) is added in (a), (b), (c) and (d). The vertical scale is normalized to the light intensity transmitted through the empty cavity. (a)  $T = 105^\circ\text{C}$ ; (b)  $T = 110^\circ\text{C}$ ; (c)  $T = 115^\circ\text{C}$ ; (d)  $T = 120^\circ\text{C}$ ; (e) The saturated absorption spectroscopy (curve 1) and the corresponding cavity transmission spectra (curve 2) of the coupled atoms-cavity system.  $T = 120^\circ\text{C}$ .

ting peaks were observed experimentally. Such multi-normal-mode peaks depend sensitively on the atomic density. This phenomenon can be qualitatively explained by using the linear absorption and dispersion theory of the cavity transmission, and by taking into account the sensitive dependence of the index of refraction of the intracavity medium on the atomic density. This work sheds new light on the investigations of this novel “superstrong coupling” region in the exciting field of collective coupling between atoms and cavity, and can lead to interesting applications in quantum information processing.

<sup>†</sup>Corresponding author’s email address: jzhang74@sxu.edu.cn, jzhang74@yahoo.com

J. Zhang thanks K. Peng, C. Xie and T. Zhang for the helpful discussions. This research was supported in part by NSFC

for Distinguished Young Scholars (Grant No. 10725416), National Basic Research Program of China (Grant No. 2006CB921101), NSFC Project for Excellent Research Team (Grant No. 60821004), and NSFC (Grant No. 60678029).

- [1] P. R. Berman, Cavity Quantum Electrodynamics (Advances in Atomic, Molecular, and Optical Physics, Academic, New York, 1994).
- [2] T. Pellizzari, S. A. Gardiner, J. I. Cirac, P. Zoller, Phys. Rev. Lett. **75**, 3788 (1995); L. M. Duan, H. J. Kimble, Phys. Rev. Lett. **92**, 127902 (2004); J. I. Cirac, P. Zoller, H. J. Kimble, H. Mabuchi, Phys. Rev. Lett. **78**, 3221 (1997).
- [3] A. Boca, R. Miller, K. M. Birnbaum, A. D. Boozer, J. McKeever, and H. J. Kimble, Phys. Rev. Lett. **93**, 233603 (2004).
- [4] P. Maunz, T. Puppe, I. Schuster, N. Syassen, P. W. H. Pinkse, and G. Rempe, Phys. Rev. Lett. **94**, 033002 (2005); T. Puppe, I. Schuster, A. Grothe, A. Kubanek, K. Murr, P. W. H. Pinkse, and G. Rempe, Phys. Rev. Lett. **99**, 013002 (2007).
- [5] M. Tavis, F. W. Cummings, Phys. Rev. **170**, 379 (1968).
- [6] G. S. Agarwal, Phys. Rev. Lett. **53**, 1732 (1984).
- [7] Y. Zhu, D. J. Gauthier, S. E. Morin, Q. Wu, H. J. Carmichael, and T. W. Mossberg, Phys. Rev. Lett. **64**, 2499 (1990).
- [8] R. J. Thompson, G. Rempe, and H. J. Kimble, Phys. Rev. Lett. **68**, 1132 (1992).
- [9] J. Klinner, M. Lindholdt, B. Nagorny, A. Hemmerich, Phys. Rev. Lett. **96**, 023002 (2006).
- [10] A. K. Tuchman, R. Long, G. Vrijsen, J. Boudet, J. Lee, and M. A. Kasevich, Phys. Rev. A **74**, 053821 (2006).
- [11] G. Hernandez, J. Zhang, and Y. Zhu, Phys. Rev. A **76**, 053814 (2007).
- [12] S. Gupta, K. L. Moore, K. W. Murch, and D. M. Stamper-Kurn, Phys. Rev. Lett. **99**, 213601 (2007); Y. Colombe, T. Steinmetz, G. Dubois, F. Linke, D. Hunger, J. Reichel, Nature **450**, 272 (2007); F. Brennecke, T. Donner, S. Ritter, T. Bourdel, M. Kohl, T. Esslinger, Nature **450**, 268 (2007).
- [13] J. Gea-Banacloche, H. Wu, and M. Xiao, Phys. Rev. A **78**, 023828 (2008).
- [14] P. Domokos and H. Ritsch, Phys. Rev. Lett. **89**, 253003 (2002); J. K. Asboth, P. Domokos, H. Ritsch, and A. Vukics, Phys. Rev. A **72**, 053417 (2005).
- [15] B. Nagorny, Th. Elsasser, A. Hemmerich, Phys. Rev. Lett. **91**, 153003 (2003); D. Kruse, C. von Cube, C. Zimmermann, and P. W. Courteille, Phys. Rev. Lett. **91**, 183601 (2003); A. T. Black, H. W. Chan, and V. Vuletic, Phys. Rev. Lett. **91**, 203001 (2003); S. Slama, S. Bux, G. Krenz, C. Zimmermann, and Ph. W. Courteille, Phys. Rev. Lett. **98**, 053603 (2007).
- [16] D. Meiser and P. Meystre, Phys. Rev. A **74**, 065801 (2006).
- [17] L. M. Duan, J. I. Cirac, P. Zoller, E. S. Polzik, Phys. Rev. Lett. **85**, 5643 (2000); L. M. Duan, G. Giedke, J. I. Cirac, P. Zoller, Phys. Rev. Lett. **84**, 4002 (2000); B. Julsgaard, A. Kozhekin, E. S. Polzik, Nature **413**, 400 (2001).
- [18] R. W. Boyd, Nonlinear Optics, (Academic, San Diego, CA, 2003).
- [19] <http://steck.us/alkalidata>.
- [20] H. Wu, J. Gea-Banacloche, and M. Xiao, Phys. Rev. Lett. **100**, 173602 (2008).